

ARTICLE

Open Access



Bfra-loaded nanoparticles confer protection against paratuberculosis infection

Yiduo Liu¹, Yulan Chen¹, Zhengmin Liang¹, Lijia Luo¹, Yuanzhi Wang¹, Haoran Wang¹, Xin Ge¹, Srinand Sreevatsan^{2*} and Xiangmei Zhou^{1*}

Abstract

Paratuberculosis is a chronic wasting disease of granulomatous enteritis in ruminants caused by *Mycobacterium avium* subsp. *paratuberculosis* (*M. paratuberculosis*, MAP) resulting in heavy economic losses to dairy industries worldwide. Currently, commercial vaccines were not effective in preventing pathogen shedding and were reported with serious side effects. To develop a novel and smarter paratuberculosis vaccine, we utilized PLGA nanoparticles encapsulating the Bfra antigen (Bfra-PLGA NPs). We observed that mice vaccinated with Bfra-PLGA NPs exhibited an enhanced secretory IFN- γ , CD4⁺ T cells response and antibody IgG against MAP infection. In addition, secretions of the inflammatory cytokine TNF- α and IL-10 were increased following treatment with Bfra-PLGA NPs. A significant reduction in bacterial load was observed in the livers and spleens of animals vaccinated with Bfra-PLGA NPs. Furthermore, Bfra-PLGA NPs were effective to alleviate the pathological lesions of livers in mice. Overall, our approach provides a rational basis for employing PLGA nanoparticles to develop improved vaccines that induced protective immunity against paratuberculosis.

Keywords *Mycobacterium avium* subsp. *paratuberculosis*, PLGA nanoparticles, Bfra, Immune responses, Novel vaccine

*Correspondence:

Srinand Sreevatsan

sreevats@msu.edu

Xiangmei Zhou

zhouxm@cau.edu.cn

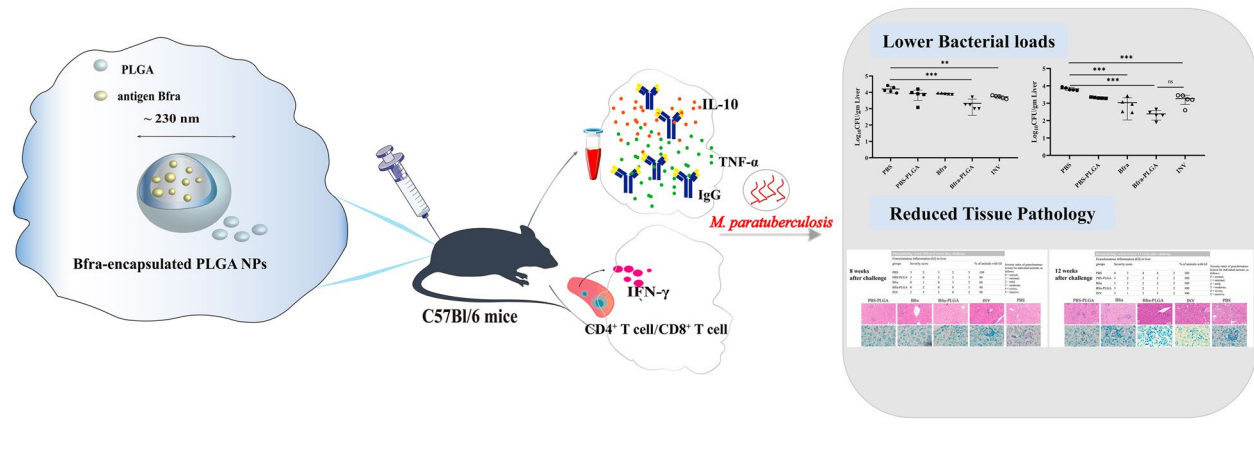
¹ College of Veterinary Medicine, National Key Laboratory of Veterinary Public Health and Safety, China Agricultural University, Beijing, China

² Pathobiology and Diagnostic Investigation College of Veterinary Medicine, Michigan State University, East Lansing, MI, USA



© The Author(s) 2023. **Open Access** This article is licensed under a Creative Commons Attribution 4.0 International License, which permits use, sharing, adaptation, distribution and reproduction in any medium or format, as long as you give appropriate credit to the original author(s) and the source, provide a link to the Creative Commons licence, and indicate if changes were made. The images or other third party material in this article are included in the article's Creative Commons licence, unless indicated otherwise in a credit line to the material. If material is not included in the article's Creative Commons licence and your intended use is not permitted by statutory regulation or exceeds the permitted use, you will need to obtain permission directly from the copyright holder. To view a copy of this licence, visit <http://creativecommons.org/licenses/by/4.0/>.

Graphical Abstract



Introduction

Paratuberculosis or Johne's disease (caused by *Mycobacterium avium* subsp. *paratuberculosis*, MAP) is an irreversible, chronic wasting disease in ruminants and has been also isolated from other non-ruminant wildlife species [1]. As an obligate intracellular bacterium, MAP can be found in macrophages throughout the body within infected animals [2]. Over the course of paratuberculosis, Th1 type immune response dominates the initial stage and then is gradually replaced by Th2 humoral immune response which is incapable of controlling the intracellular infection at this point [3, 4]. Then, the symptoms of paratuberculosis become apparent including chronic hyperplastic enteritis, intractable diarrhea, intestinal mucosa thickening and forming folds, weight loss, decreased milk production, fertility and other symptoms, resulting in the reduction of animal performance and economic losses [5]. It has been estimated that the impact of lower milk production due to MAP infections on America economy is US\$200 million \pm US\$160 million per year [5–7].

MAP does not only seriously affect the development of animal husbandry, but also poses a threat to human health. Crohn's disease (CD) is a chronic inflammatory bowel disease with unknown etiology, while there is evidence linking MAP and CD [8]. Cases were reported that viable MAP was identified from breast milk and peripheral blood from CD patients [9, 10]. In addition, the primary symptoms of Crohn's disease are persistent diarrhea and intestinal fistula, which are clinically similar to the symptoms of paratuberculosis. Beyond Crohn's disease, MAP is associated with many inflammatory and autoimmune disorders including type I diabetes, multiple sclerosis (MS), granulomatous arthritis in children (Blau

syndrome), and rheumatoid arthritis [11–13]. MAP can be cultured from the milk and other dairy products of cattle with both clinical and subclinical Johne's disease, which are the most plausible candidates as vehicles of transmission of MAP from cattle to humans [14–16]. As moderately higher existence of anti-MAP antibodies in population was reported, there is an urgent need for measures to control and intervene the MAP-load in animals and the environment [17].

Due to the economic costs, impacts on animal welfare and aroused public health concerns caused by paratuberculosis, it is vital to develop control strategies and screen for relevant antigens to introduce them as candidate vaccines. The performance of the existing vaccines for paratuberculosis (Gudair[®], Silirum[®], and Mycopar[®]) are effective in controlling disease, but none limit disease spread and can cause adverse reactions [18, 19]. Given the challenges to control JD with the current vaccine, we developed a novel subunit vaccine with MAP antigen Bfra delivered by poly (lactide-co-glycolide) (PLGA). PLGA has been approved by the Food and Drug Administration (FDA) as a delivery vehicle for vaccines and drugs due to its biocompatibility, non-immunogenicity, antigen stabilization, controlled and sustained antigen release in humans and animals [20, 21]. PLGA-based vaccines can shield the loaded peptides/proteins against proteolytic degradation and show a suitable plasma half-life [22]. According to research, PLGA is an ideal delivery carrier for pathogen-specific antigens in subunit vaccines against several diseases including HIV, tuberculosis and influenza [23–27].

Bfra, named as Antigen D of MAP, can enrich, manage and store iron ions, maintain the balance of intracellular iron ions so as to enhance the viability of MAP [28].

Bfra has been reported as a T-cell antigen that can induce IFN- γ expression and lymphocyte proliferation [29]. In addition, immunizing mice with DNA vaccines encoding Bfra and recombinant protein Bfra can induce an evident humoral immune response, and thus have certain protective effects on mice from *Brucella abortus* infection [30]. Moreover, Bfra antigen of *Brucella melitensis* mixed with adjuvant CpG ODN was able to induce the humoral and cellular immune responses in mice [31].

Considering these concerns, we conducted the study to explore the potential of Bfra encapsulated PLGA NPs against MAP infection in mice. Our results demonstrated that Bfra-NPs vaccination induced cell-mediated immune response and also elicited humoral immune response against MAP, resulting in a reduced pathological lesions and bacterial burden in the spleens and livers of infected mice. In conclusion, the nanoparticles candidate vaccine demonstrates a good protection from MAP infection.

Results

Characterization of Bfra-PLGA NPs

Recombinant Bfra protein was expressed in *Escherichia coli* and was purified by Ni-NTA column as described in Methods. The purified recombinant Bfra antigen was

confirmed by western-blotting using anti-His monoclonal antibody and SDS-PAGE after Coomassie brilliant blue staining (Fig. 1 A and B). To determine the encapsulation of recombinant Bfra protein, we dissolved the Bfra-PLGA NPs by NaOH-based extraction method. Western blotting with an anti-His monoclonal antibody validated the protein loading (Fig. 1A). The current study used double-emulsion solvent evaporation to create PLGA NPs encapsulating Bfra. Scanning electron photomicrographs of Bfra-PLGA NPs revealed a homogeneous, spherical and smooth appearance (Fig. 1C and D). Dynamic light scattering of a Bfra-PLGA NPs suspension on the Malvern Zetasizer indicated narrow size distribution and greater colloidal stability (Fig. 1 E and F). According to Malvern Zetasizer, the average size of Bfra-NPs was 230 ± 6.48 nm with a polydispersity index (PDI) of 0.153 (< 0.2), indicating negligible NPs heterogeneity. In addition, the zeta potential of Bfra-PLGA NPs was -21.2 ± 7.21 mV. Moreover, we conducted an experiment on the particle size change over a week to test the stability of NPs by Malvern Zetasizer and the size of Bfra-NPs changed gently within a week (Fig. S1). To estimate the release of Bfra at physiological pH and within macrophages pH, the amount of Bfra encapsulated were measured at various time points over 10 days' time period. A sudden release was observed

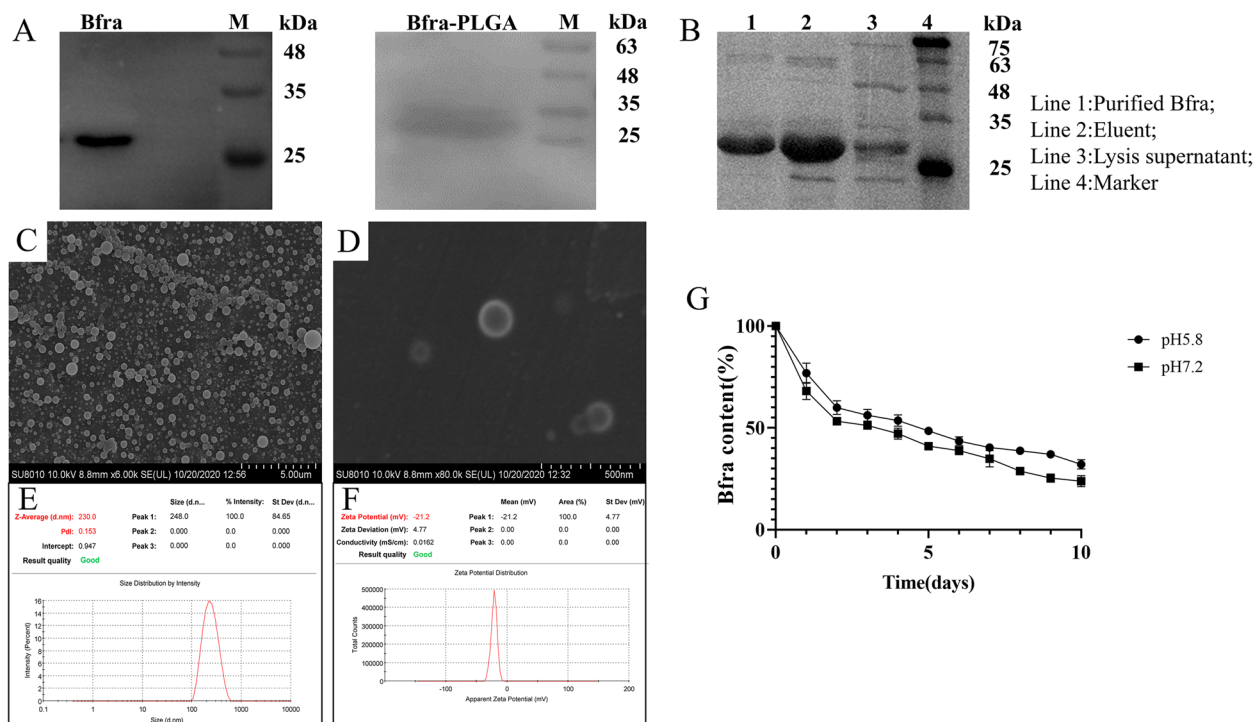


Fig. 1 Preparation and characterization of Bfra NPs. **A** Western blotting with an anti-His monoclonal antibody confirmed the recombinant Bfra protein and protein retrieved from Bfra-PLGA NPs. **B** Purified recombinant Bfra was ~ 30 kDa, as measured by SDS-PAGE. **C** Scanning Electron Microscope (SEM) at magnifications of (C) $\times 6$ k and **D** $\times 80$ k for Bfra-NPs. **E** Average size and **F** potential of Bfra-NPs. **G** Residual Bfra (%) within Bfra-NPs at pH 7.4 and 5.8 was measured by BCA over 10 days' time period

on the first day, while an increased release was observed gently with a time period at both pH (Fig. 1G).

Meanwhile, to estimate the encapsulation efficiency, we obtained the supernatant. Using a BCA kit, the result revealed that the encapsulation efficiency of Bfra-NPs was determined to be 71%, while the loading efficiency was 1.6%.

Cytotoxicity and uptake of NPs by macrophages

The MTS assay was performed to test the influence of Bfra-NPs on viability of macrophages. As shown in Fig. 2A, The result revealed that Bfra-PLGA NPs were nontoxic to RAW264.7 cells at 100 µg/mL. Therefore, we selected 100 µg/ml as a nontoxic dose for in vitro investigations. The immunological features of PLGA NPs are dictated by their specific physicochemical composition, which promotes antigen uptake and redirection to lymphoid organs. Based on the inherent property of NPs, RAW264.7 cells were cultured under ex vivo conditions to assess macrophages’ ability to phagocytose Bfra-NPs. We treated RAW264.7 cells with Bfra-NPs for up to 6 h to investigate the uptake of NPs by macrophages. According to the microscopy, we found that FITC-labeled Bfra antigens can be observed inside the macrophages (Fig. 2B). After 2 h of incubation, FITC-labeled Bfra antigens can be seen inside the macrophages, indicating that Bfra-NPs

can be internalized by macrophages. Upon 6 h, the FITC fluorescence signal was detected inside 80% of the macrophages. These results suggest that Bfra-NPs have the potential to induce the activation of macrophages and to be efficiently taken up by APCs. In addition we confirmed the stability of Bfra antigen encapsulated in NPs which were uptaken by macrophage after 6 h by western-blotting (Fig. S2).

Immune responses induced by Bfra-NPs before challenge in mice

Before the formal experiment, we conducted a histopathological study of mice treated with Bfra-NPs to detect toxicity of NPs in vivo. According to histopathological observation, there were no pathological changes in lung, spleen, liver and kidney tissues of mice in all treated groups (Fig. S3).

Following an immunization protocol as described in Fig. 3, we collected serum and spleen samples from mice after 2 weeks of third boosting immunization. As expected, all immunized mice elicited significantly increased IL-10 and TNF-α levels compared to PBS treated mice (Fig. 4A and B). The IgG antibody titers of serum were also measured to assess the immune responses induced by Bfra-NPs. Similarly, we found that a significantly higher response of IgG antibody

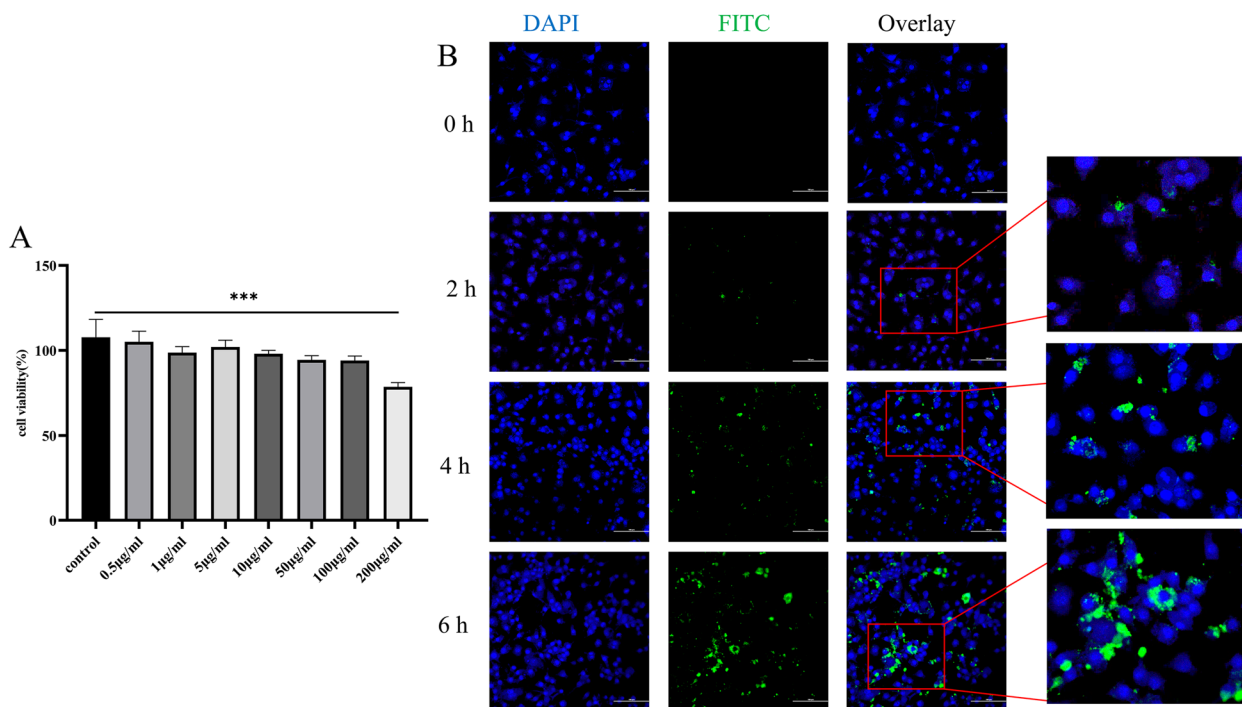
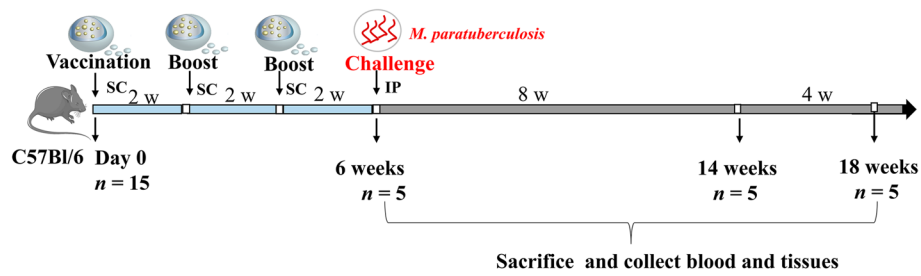


Fig. 2 Cytotoxicity and confocal analysis of Bfra-FITC NPs internalization by macrophages. **A** Cell viability of RAW264.7 macrophages exposed to Bfra-PLGA NPs after 24 h. **B** The macrophages were stained with DAPI (tracers for cell nucleus staining) and Bfra was labeled with FITC. Bfra-PLGA NPs were internalized within 6 h and images were visualized at 400× magnification. Scale Bar: 100 µm



Immune dose (sc): 100 µg Bfra protein/mouse
 75 µg Bfra encapsulated in 5 mg PLGA NPs/mouse
 inactivated MAP strain K-10 (10⁶ CFU/mouse)
Challenge dose (ip): 10⁸ CFU MAP 2015WD-1

Fig. 3 Experimental design for vaccination and challenge. Female C57BL/6 mice (6-8 weeks old) were subcutaneously vaccinated and then intraperitoneally challenged with a virulent strain of MAP 2015WD-1 two weeks later. At various times, mice (n = 5/group) were slaughtered. Tissue and blood samples were taken to determine the bacterial burden, cytokine levels, and histopathology

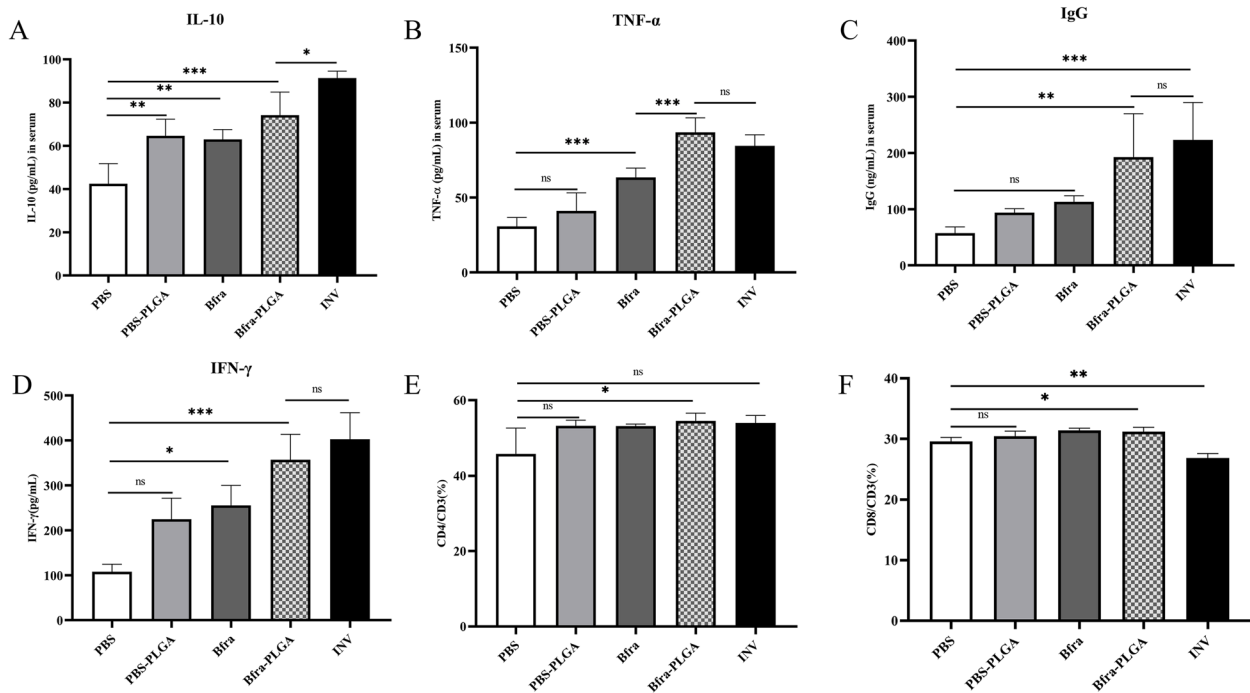


Fig. 4 Analysis of immune responses in immunized mice before challenge. Mice (n=5) from each group were euthanized 2 weeks post-immunization to analyze the immune response. ELISA was used to detect **A** IL-10, **B** TNF-α, and **C** IgG in serum samples. Splenocytes were extracted and activated in vitro with Bfra to assess **D** IFN-γ. The graph of **E** CD4⁺ T cells and **F** CD8⁺ T cells in post-immunization spleen tissue of mice. A asterisk denotes a statistically significant difference: *p < 0.05, **p < 0.01, and ***p < 0.001

in Bfra-PLGA treated mice compared to other groups except inactivated MAP strain K-10 treated group (Fig. 4C).

Spleen samples were collected to prepare single cell suspension for the evaluation of cell mediated immune response. Splenocytes were stimulated with Bfra for 24 h to determine the level of IFN-γ produced. As shown in

Fig. 4D, the IFN-γ production in Bfra-PLGA treated mice was significantly higher than other groups except the inactivated vaccine. We also analyzed the T cell repertoire stimulated with the NPs by flow cytometry (Fig. 4E and F). The frequency of CD4⁺ T cells was higher in almost all vaccinated mice compared to PBS treated mice while significant differences was only observed in

Bfra-PLGA treated group (Fig. 4E). According to Fig. 4F, the frequency of CD8⁺ T cells in Bfra and Bfra-NPs treated mice were significantly higher compared to other groups, while we observed a significant reduced frequency in inactivated vaccine group.

Collectively, these results indicated that Bfra-NPs induced strong humoral immune response and cell-mediated immune response in mice.

Protection induced by Bfra-NPs after challenge by MAP

Mice were challenged with *M. paratuberculosis* field isolate strain 2015 WD-1 after 2 weeks of receiving the third boosting dose of vaccination to assess the protective effect of Bfra-NPs. In order to investigate whether Bfra-NPs were beneficial for reducing weight loss in animals, we recorded total body weight of mice on weekly basis post infection with *M. paratuberculosis* (Fig. S4). We observed a mark reduction in total body weight at 10th week post infection in all experimental groups, while the PBS treated mice consistently gained less weight than the other groups. After 8 and 12 weeks of infection, the mice were sacrificed.

At 8 weeks post challenge, the bacterial load in the livers of Bfra-NPs and inactivated MAP vaccinated groups was significantly reduced compared to other groups. In contrast, the latter demonstrated a lower bacterial load (Fig. 5A). Furthermore, the bacterial load in spleens of Bfra and Bfra-NPs vaccinated groups showed significant reduction compared to other groups (Fig. 5B). In addition to bacterial colonization, organ coefficients of livers

and spleens were also measured. According to Fig. 5C and D, significantly low spleen weight were observed in Bfra-NPs treated mice compared with inactive vaccine, while there were no significant differences of liver coefficients among all groups.

At 12 weeks post-challenge, significant reductions of bacterial load both in livers and spleens were observed in all vaccinated groups compared to PBS treated group (Fig. 5E and F). As expected, the Bfra-NPs produced more effective protection of the bacterial load in livers and spleens. There were similar results of organ coefficients, while the PBS treated mice showed significantly heavier liver weight in comparison with vaccinated groups (Fig. 5G and H). Collectively, vaccination with the antigen Bfra and Bfra-PLGA NPs reduced bacterial burden in mice generated by the challenge with virulent strain of *M. paratuberculosis*.

Histopathological analysis for the immuned mice challenged by MAP

We performed histopathology studies in all groups to measure the degree of pathological damage and to detect bacterial dispersion in mice tissue. At 8 weeks post challenge, all PBS treated mice had granulomatous inflammation in the liver, whereas only 40% of the animals receiving the Bfra-PLGA vaccine exhibited inflammation (Fig. 6A and B). As we expected, histopathological score of the Bfra-NPs group was lower than other groups. Surprisingly, 90% of the mice vaccinated the inactivated vaccine exhibited mild to moderate pathological changes.

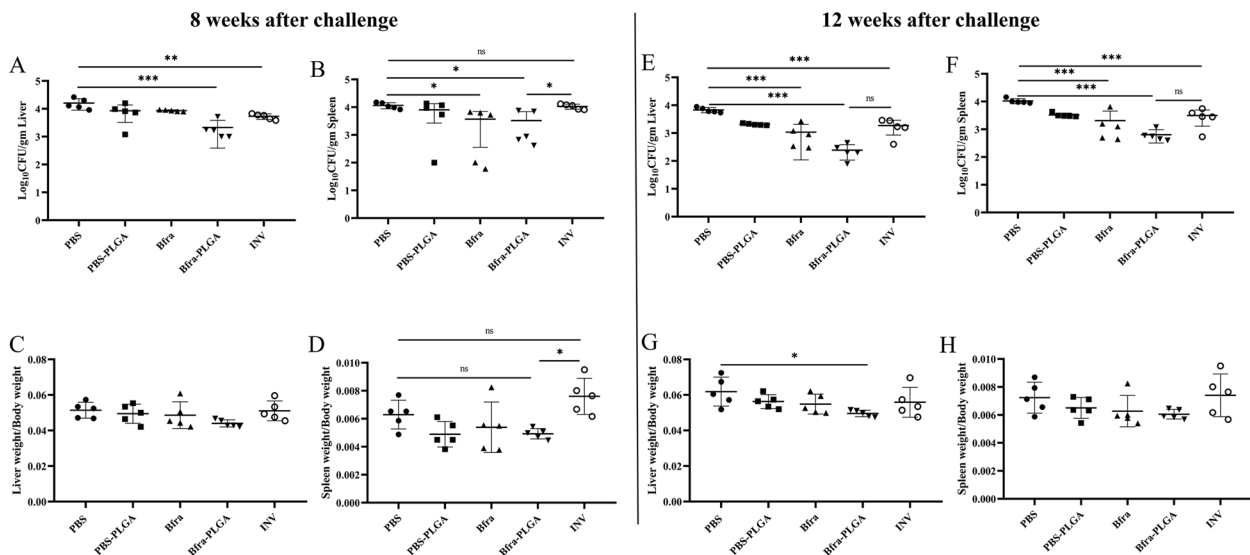


Fig. 5 Protection against challenge strain of *M. paratuberculosis*. Following challenge, mice groups ($n=5$) were sacrificed at 8 weeks after challenge and bacterial burden was analyzed in liver **A** and spleen **B** organs. The proportion of liver **C** and spleen **D** weight to total body weight was analyzed at 8 weeks after MAP infection. Following the challenge, mice groups ($n=5$) were sacrificed at 12 weeks after the challenge, and bacterial burden was analyzed in the liver **E** and spleen **F** organs. The proportion of liver **G** and spleen **H** weight to total body weight was analyzed 12 weeks after MAP infection. A sterisk refers to statistical significant difference, $*p < 0.05$, $**p < 0.01$, and $***p < 0.001$

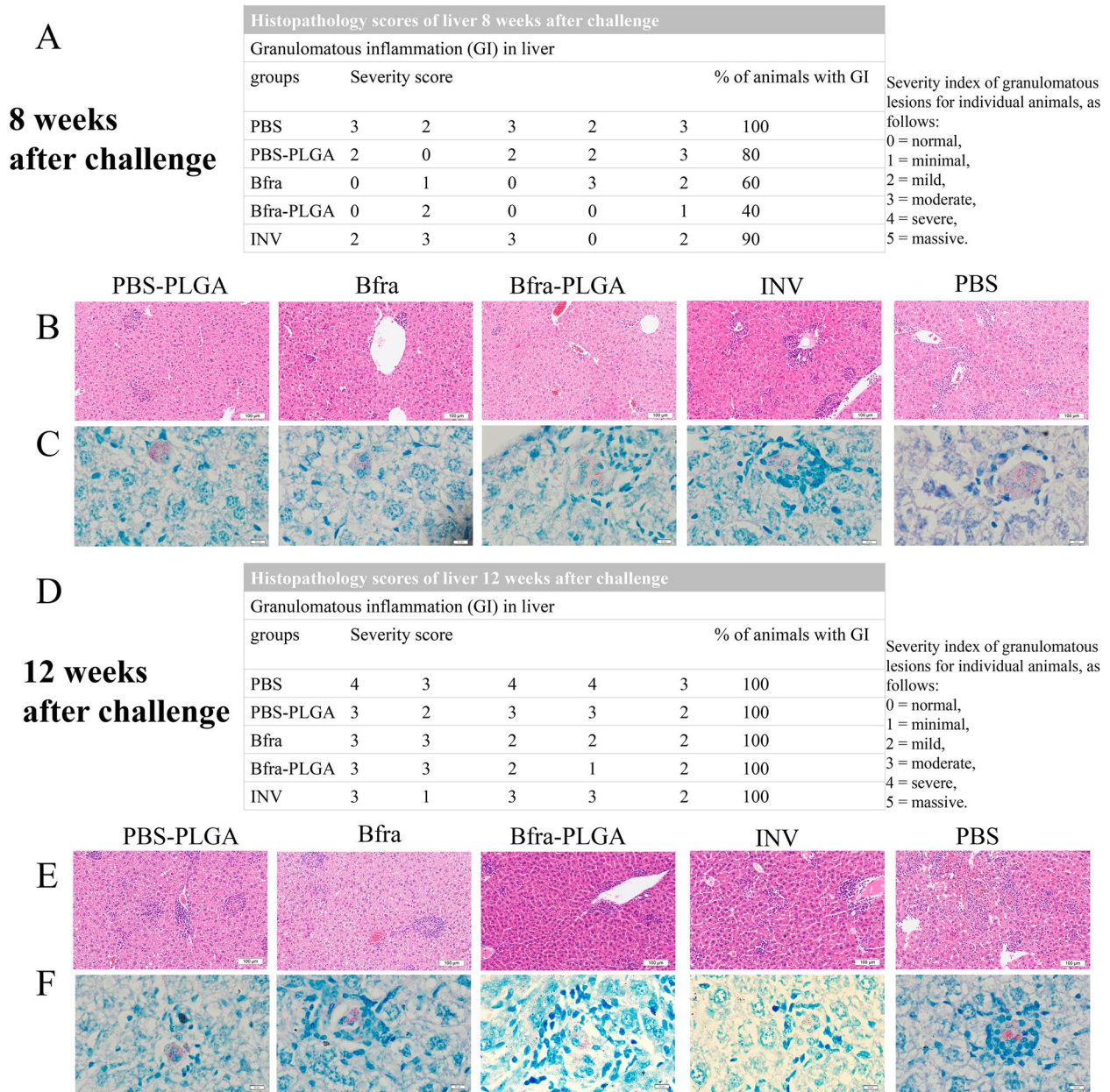


Fig. 6 Histopathology analysis of livers after infection. Following challenge, mice groups ($n=5$) were sacrificed at 8 weeks after challenge. Tissues were sectioned to 5 μm slices and stained. Slides were scored by a trained pathologist blinded to the samples **A**. Representative images of H&E stained livers of mice **B**. Representative images of AFS stained livers of mice **C**. The mice groups ($n=5$) were sacrificed at 12 weeks after the challenge. Tissues were sectioned into 5 μm slices and stained. Slides were scored by a trained pathologist blinded to the samples **D**. Representative images of H&E stained livers of mice **E**. Representative images of AFS stained livers of mice **F**

In addition, using acid-fast staining (AFS) method, we found acid-fast bacillus in livers of all group under microscope (Fig. 6C). At 12 weeks post-challenge, all mice tested developed granulomatous inflammation in the liver, with the Bfra-NPs group having a lower histological score than the other groups (Fig. 6D). Unsurprisingly, there is an extensive infiltration of inflammatory cells in

some livers of mice treated only with PBS, while the liver lesions in other groups were mainly localized inflammatory foci (Fig. 6E). Same as above, acid-fast bacilli were also observed in livers at 12 weeks post-challenge for all groups (Fig. 6F). Taken together, these findings suggest that Bfra-PLGA NPs can reduced tissue pathological changes in mice infected with *M. paratuberculosis*.

Discussion

Since the negative impact and threat of MAP on livestock development, economy and public health, rational control strategies are necessary [32]. Vaccination is an excellent option for controlling the disease at a low cost. The current commercial MAP vaccines are inactivated or attenuated MAP incorporated into water-in-oil emulsions while serious reactions to the adjuvant have been reported and limited protection provided by these vaccines against bacterial tissue colonization and shedding. Previous studies have shown that subunit vaccines have the advantage of reducing the possibility of infections that may be produced by live attenuated vaccines [33, 34]. And it has been revealed that there is a need to combine subunit vaccine with efficient adjuvants to improve the immunogenicity [34]. Considering these issues, we encapsulated MAP specific antigen Bfra to PLGA nanoparticles.

In the present study, we evaluated the potential of Bfra-encapsulated PLGA NPs as a vaccine compared to inactivated MAP strain K-10 in protection against paratuberculosis. Antigen encapsulated in PLGA can be released sustainly and slowly so as to provide more effective MHC peptide complexes presentation to CD8⁺ T cells which is essential to stimulate effective immune responses [35, 36]. There are some factors influencing encapsulated protein release such as particle size, surface structure and morphology [37]. Studies indicate that PLGA in the nanometer range (size 200–500 nm) causes superior TH1-response and can be better taken up by DCs to lymph nodes 24 h after administration [22]. The resultant NPs in our study were 230 ± 6.48 nm, further encouraging their absorption by DCs and the activation of Th1-response. Alongside size, the Bfra-NPs had a smooth surface and a spherical form, indicating that they are better antigen carriers.

MAP is a typical intracellular pathogen, which mainly survived in macrophages [38]. In the process of MAP infection and recovery, cellular immunity play a crucial role in clearing MAP, particularly Th1-type responses represented by CD4⁺ T cells [39]. It is generally believed that Th1 immune response is dominant in the early stage of MAP infection, but there is a conversion of Th1 to Th2 immune response in the subclinical and clinical stages [40, 41]. In the present study, we analyzed the levels of IFN- γ (Th1), TNF- α (Th1) and IL-10 (Th2). Both the secretion of IFN- γ and TNF- α are enhanced in the Bfra-NPs group. IFN- γ is a Th1 cytokine, that can promote the activation and proliferation of T cells and activate macrophages to clear intracellular pathogens [42, 43]. In line with previous findings, the enhanced secretion of inflammatory cytokine TNF- α has been attributed to the potential role played by PLGA NPs in NF κ B translocation to the cell nucleus [44].

In addition, our experiment found that, the frequency of CD4⁺T cells and CD8⁺T cells was significantly enhanced in Bfra-NPs-vaccinated mice. These data imply that Bfra-NPs can trigger a enhanced TH1 response which provide a rational explanation for enhanced T cell proliferation in mice. We also found a elevated level of IL-10 in Bfra-NPs immunized mice. IL-10 is a Th2 bias cytokine while a recent study shows that, Th1 cells co-expressing IL-10 are more conducive in clearing intracellular pathogens [45]. Alongside enhanced cellular immunity, the results showed that the secretions of IgG were significantly increased in the Bfra-PLGA NPs group, proving that the NPs could enhance the humoral immunity of mice. Generally, our data indicated that the Bfra-PLGA NPs conferred an acceptable immune response especially Th1 immunity. Since we observed enhanced levels of cytokines and proliferation of CD4⁺ T cells and CD8⁺ T cells in the Bfra-PLGA group, this provides a possible explanation for the enhanced protection against MAP infection. Interestingly, we found a similar activated immune response in the inactivated vaccine group except the decreased proliferation of CD8⁺ T cells.

As we expected, lower bacterial burden of livers were observed in both Bfra-PLGA and inactivated vaccine immunized mice at 8 weeks after challenge. Respectively, in the experiment, a significant reduction of the bacteria load in spleen was only observed in Bfra-PLGA NPs treated mice at 8 weeks after MAP infection. Thus, we hypothesize that the superior protective effect of Bfra-NPs over the inactivated vaccine is attributed to the robust CD8⁺ T cells proliferation. Moreover, we suprisingly found that Bfra, Bfra-PLGA and inactivated MAP strain K-10 were sufficient to reduce tissue bacteria colonization at 12 weeks after infection compared to the control group. The correlates of protective effect observed among immunized groups were further asserted by histological lesions. Compared to the other immunized group, the Bfra-PLGA NPs were sufficient to reduce lesion scores in mice. Persistent diarrhea and emaciation are important clinical features of paratuberculosis. In our study, immunization produced higher weight gain following the challenge than the non-immunized group. Overall, these data suggest that Bfra can be regarded as a specific antigens for MAP vaccines and PLGA NPs can be an adjuvant as well as a rational delivery system.

As a major iron storage protein, Bfra which exists widely in bacteria plays the dominant role in regulating the balance of iron metabolism and resisting the toxicity of nitrogen peroxide to bacteria [46–48]. According to a study, the levels of antibodies against Bfra were elevated in 53% Crohn's disease patients, indicating the superior immunogenicity of Bfra [49]. A recent study

have shown that Bfra is a major antigen of *S. pullorum* and Bfra induced IFN- β expression via the p38 MAP Kinase signaling pathway in cells [50]. IFN- β is reported as an important congenital immunity cytokine mediating expression of hundreds of IFN-stimulated genes (ISGs) to resist pathogens [51, 52]. Moreover, considering the immunogenicity of Bfra demonstrated in our study, we can assume that Bfra effectively activates both innate immunity (IFN- β) and adaptive immunity. Given the side effects of conventional oil emulsion adjuvant and weak uptake of antigens and in vivo degradation, we used PLGA NPs as delivery vesicles or prospective adjuvants. Consistent with previous studies, we found PLGA-delivered antigen Bfra could promote immune response and provide effective protection against *M. paratuberculosis* infection. Encouragingly, the Bfra-PLGA NPs can diminish hepatic pathological lesions in mice.

Vaccines for animals, based on the One-Health philosophy, play a positive and vital role in maintaining the health and welfare of companion and economic animals and preventing disease transmission. With the increasing concern for paratuberculosis, there has been an increase in the development of new technologies such as attenuated vaccines and virus vector vaccines against PTB [53–55]. However, the two approaches are controversial, particularly arising certain problems about safety and the return of virulence. The combination of subunit vaccines with NPs can improve the immune efficacy of antigens while avoiding these limitations. In our study, the PLGA-based paratuberculosis nanovaccine was highly immunogenic and performed effectively against *M. paratuberculosis* infection in mouse models. Furthermore, no adverse reactions were observed at the injection location. It should be noted that recombinant antigen Bfra were able to impart superior protective immunity against *M. paratuberculosis* challenge in this study. Future research will focus on identifying the immunological mechanism(s) responsible for the activity of Bfra-PLGA NPs and modifying the method of distribution to improve the vaccination efficacy of NPs.

Materials and methods

Bacteria and culture conditions

Cultures of MAP strains were prepared from single colonies in Middlebrook 7H9 broth (Difco, BD biosciences, USA) supplemented with 10% ADC (albumin, dextrose, catalase), 2 μ g/mL mycobactin J (Allied Monitor, MO, USA), and 0.05% Tween 80 (Sigma-Aldrich Crop., CA, USA). *M. paratuberculosis* K-10 was inactivated in a water bath at 80 °C for 30 min to prepare the inactivated vaccine while *M. paratuberculosis* field isolate strain 2015WD-1 was prepared for mice infection [56]. Recombinant *Escherichia coli* (*E. coli*) strains were cultured in

Luria–Bertani broth (BD) under standard conditions. All cultures were cultivated at 37 °C with shaking at 180 rpm until they reached the log phase.

Preparation of PLGA-encapsulated Bfra NPs

The full length Bfra with 6 \times His-tag was expressed by pET-30a(+) vector plasmid in *Escherichia coli* BL21 cells. Then, the recombinant protein Bfra was purified on a Ni–NTA column from lysate supernatant of the recombinant *E. coli*. The 6 \times His-tagged Bfra was confirmed by SDS-PAGE and western-blotting using anti-His monoclonal antibody.

PLGA nanoparticles (L/G is 50:50, Mw: 10 KDa, Jinan Daigang Biomaterial Co., Ltd, Shandong, China) encapsulated protein were prepared by the double emulsion water-in-oil-in-water (W/O/W) method. Firstly, the primary emulsion was generated by sonication (240 W, 6 min) (Scientz, Zhenjiang, China) of an internal aqueous phase containing protein (2 mg/mL) and an organic phase (30 mg/mL PLGA) in ethyl acetate (EtAc, Innochem Co., Beijing, China). The resulting water-in-oil (wi/o) emulsion was then added to 10 mL PVA (1% w/v) (Innochem Co., Beijing, China) and emulsified in an ice-water bath to form the double emulsion (w/o/w). The emulsifications were performed using probe sonicator set at 360 W of energy output for 8 min in an ice bath. The double emulsion (w/o/w) was diluted in 10 mL PVA (0.5% w/v) solution and the emulsion was agitated 4–6 h to allow the organic phase to evaporate. Then, the NPs were collected by centrifugation at 10,000 rpm for 5 min to remove the remaining PVA and purified with distilled water three times. Finally, all NPs were lyophilized.

The physicochemical characterization of NPs

To evaluate the encapsulation efficiency (EE) and loading efficiency (LE) of the NPs, we measured the protein encapsulated using a BCA protein-assay kit (Beyotime Institute of Biotechnology, Beijing, China) by NaOH based extraction method. In brief, 1 mL NaOH (1 M) were added to dissolve 10 mg NPs, followed by incubation at 37 °C for 18 h under constant shaking. Then, we added HCl for neutralization followed by centrifugation at 12,000 g for 10 min. The resulting supernatant was estimated by BCA method using BSA standards. Protein integrity was confirmed by western-blotting using anti-His monoclonal antibody.

$$EE\% = \frac{\text{amount of Bfra released from NPs}}{\text{amount of Bfra in the internal aqueous phase}} \times 100\%$$

$$LC\% = \frac{\text{amount of Bfra released from NPs}}{\text{amount of NPs}} \times 100\%$$

Particle size range, polydispersity index and zeta potential were measured by dynamic light scattering (DLS) using a Malvern Zetasizer Nano-ZS (Malvern Instruments, Malvern, UK). The suspensions of NPs were vortexed before analysis, and each sample was measured in triplicates. Surface morphology of the NPs was observed by scanning electron microscopy (SEM, HITACHI, Japan).

In vitro protein release curve of Bfra-NPs in pH 5.8 (phagosomal pH of macrophages) and pH 7.2 (physiological pH) for up to 10 days was estimated as described previously [57]. To test the stability of Bfra-NPs, particle size range were measured by dynamic light scattering (DLS) using a Malvern Zetasizer Nano-ZS (Malvern Instruments, Malvern, UK) for up to 7 days.

Cell viability assay

In the current study, we investigated the effect of Bfra-PLGA NPs on the viability of RAW264.7 cells by MTS method. Briefly, RAW264.7 cells were seeded into 96-well culture plates and cultured overnight. Following incubation and removal of non-adherent cells, variable concentrations of NPs ranging from 0.5 µg/mL to 200 µg/mL in medium (HyClone, Utah, USA) were added. After 24 h of incubation at 37 °C, 10 µL of MTS reactant (Promega Co., Beijing, China) was added into each well in order to assess cells susceptibility. The colorimetric density of the plate was measured by using a Microplate Reader at 570 nm.

Uptake of NPs by macrophages

To test the uptake of NPs by macrophages, we tagged the loading protein with fluorescein isothiocyanate (FITC). In the current study, we used RAW264.7 cells obtained from cold storage (National Infrastructure of Cell Line Resource, Beijing, China). The cells were cultured overnight in 24-well culture plates with DMEM medium + 10% FBS. After that, PLGA-encapsulated Bfra-FITC NPs were added to the culture at a final concentration of 0.1 mg/mL and incubated for a maximum of 6 h. Then, the culture were removed and cells were washed with sterile PBS and preserved with 2% paraformaldehyde. To observe the cellular morphology, we stained the macrophages with DAPI. Confocal images were captured using a Nikon Eclipse 80i fluorescent microscope with DAPI (blue) and FITC (green) channels and then analyzed with NIS Elements software.

Mice vaccination and infection of MAP

Specific pathogen-free (SPF) C57BL/6 J female mice (6–8 weeks old) were maintained in individually ventilated cages (IVC) (Suzhou monkey animal experimentation equipment Technology Co., Ltd, Zhejiang,

China) in BSL-2 laboratory and were randomly divided into groups. Mice were vaccinated and challenged as shown in Fig. 3. Mouse groups ($n=15$ mice/group) were immunized with PBS, PBS-PLGA, Bfra, Bfra-PLGA or inactivated MAP strain K-10 (10^6 CFU/animal) three times, 2 week apart using subcutaneous (S/C) injections. After 2 weeks of third boosting dose of immunization animals were infected with 10^8 CFU of *M. paratuberculosis* 2015WD-1 via intraperitoneal route (i.p). To evaluate the immune response and bacterial tissue colonization, mice were sacrificed 2 weeks after the third boosting dose ($n=5$ mice/group) and 8 or 12 weeks ($n=5$ mice/group) after challenge with *M. paratuberculosis* 2015WD-1 as planned for the murine model of paratuberculosis. All animal procedures were approved by the Laboratory Animal Ethical Committee of China Agricultural University (AW91110202-2) and strictly conducted by Chinese laws and guidelines.

ELISA for cytokine and IgG antibody analysis

Whole blood samples were collected at the same time as tissue collection. Blood was allowed to clot and the serum was collected after centrifugation. The ELISA technique (Neobioscience Co., Beijing, China) was used to assess IgG antibody, TNF- α , and IL-10 cytokine levels in mouse serum samples as per the manufacturer's instructions. A suspension of splenic lymphocytes was generated for the measurement of IFN- γ production by splenocytes after aseptically extracting mouse spleens and lysis of erythrocytes with the lysis buffer (ammonium chloride). Then, 5×10^6 splenocytes were seeded in 24-well cell culture plates and cultured for 24 h at 37 °C in a humidified CO₂ incubator with 10 µg/mL of Bfra protein. According to the instructions of the manufacturer, splenocyte supernatant was utilized to detect IFN- γ by ELISA (Neobioscience Co., Beijing, China).

Flow cytometry

Splenocytes from five individual mice per group were prepared for the detection of T cells population by flow cytometry assay. Single cell suspension of splenocytes were prepared as described above and were stained with fluorochrome labeled antibodies for anti-CD3 (Anti-Mouse CD3e PerCP-Cyanine5.5), anti-CD4 (anti-mouse CD4 FITC), and anti-CD8 (Anti-Mouse CD8a APC) from Multi Sciences LTD (Zhejiang, China). Cells were analyzed with BD FACSVerser™ flow cytometer (BD Biosciences, USA) and FlowJo software v10.

Protection induced by Bfra-PLGA NPs

Bacterial tissue colonization and histopathological studies were carried out for various organs of mice challenged with *M. paratuberculosis* to analyze the protection effect

of Bfra-PLGA NPs. For quantification of viable MAP bacilli in infected mice, the liver, spleen and intestinal tissues were collected for bacterio-logical and histological analysis as detailed before. The tissue homogenates were serially diluted in PBS then plated on Middlebrook 7H10 (BD diagnostic systems) supplemented with with mycobactin-J, OADC and sodium pyruvate. The plates were then incubated at 37 °C until colonies were visible. Tissues were preserved in a 10% formaldehyde solution, embedded in paraffin, cut into sections, and placed on glass slides for histopathology. After mounting, the tissues were either stained with: hematoxylin and eosin (H&E) or Ziehl–Neelsen (ZN) for the detection of acid-fast bacilli (AFB). All tissues were scored on a scale of 0 to 5 based on lesion severity per field.

Statistical analysis

Statistical analysis was performed using GraphPad Prism 5 (GraphPad Software, Inc., CA, USA). Data were analyzed using one-way ANOVA followed by Tukey's multiple comparison. Results with P values < 0.05 or better were considered significant. All research reported here was conducted in accordance with all relevant guidelines and procedures.

Supplementary Information

The online version contains supplementary material available at <https://doi.org/10.1186/s44280-023-00019-7>.

Additional file 1: Fig. S1. Stability of Bfra-NPs tested by sizechange.

Additional file 2: Fig. S2. Stability of Bfra.

Additional file 3: Fig. S3. Pathological observation of organs in mice after treated with NPs (H.E. 400x).

Additional file 4: Fig. S4. Weight changes in mice after infection.

Acknowledgements

We thank China Agricultural University for providing the Biosafety Level-2 Laboratories for experiments. This work was supported by "National Key Research and Development Program (Project No. 2021YFD1800405)"; "National Natural Science Foundation of China (Project No. 31873005, No.32172800)"; "China Agriculture Research System (No. CARS-36)".

Authors' contributions

Y.L.: Formal analysis, Investigation, Writing—original draft. Y.C.: Formal analysis, Investigation, Writing—review & editing. Z.L., L.L., Y.W., H.W., X.G.: Investigation. S.S.: Writing—review & editing. X.Z.: Conceptualization, Methodology, Funding acquisition, Writing—review & editing.

Availability of data and materials

The data shown in this paper are available in the article and its Supplementary data files or available from the authors upon request.

Declarations

Ethics approval and consent to participate

All experiments protocols and procedures were carried out according to the protocols for the care of laboratory animals, Ministry of Science and Technology People's Republic of China, and approved according to animal care and use committee (IACUC) protocols (20,110,611–01) at the China

Agricultural University, Beijing. Animal experiments proposal was approved by The Laboratory Animal Ethical Committee of China Agricultural University (AW91110202-2).

Competing interests

Author Srinand Sreevatsan is a member of the Editorial Board for One Health Advances. He was not involved in the journal's review and decisions related to this manuscript.

Received: 17 March 2023 Revised: 23 June 2023 Accepted: 29 June 2023
Published online: 03 August 2023

References

- Harris NB, Barletta RG. *Mycobacterium avium* subsp. *paratuberculosis* in Veterinary Medicine. *Clin Microbiol Rev.* 2001;14(3):489–512.
- Alonso-Hearn M, Abendano N, Ruvira MA, Aznar R, Landin M, Juste RA. *Mycobacterium avium* subsp. *paratuberculosis* (Map) fatty acids profile is strain-dependent and changes upon host macrophages infection. *Front Cell Infect Microbiol.* 2017;7:89.
- Stabel JR. Transitions in immune responses to *Mycobacterium paratuberculosis*. *Vet Microbiol.* 2000;77:465–73.
- Coussens PM, Verman N, Coussens MA, Elftman MD, McNulty AM. Cytokine gene expression in peripheral blood mononuclear cells and tissues of cattle infected with *Mycobacterium avium* subsp. *paratuberculosis*: evidence for an inherent proinflammatory gene expression pattern. *Infect Immun.* 2004;72(3):1409–22.
- Whittington R, Donat K, Weber MF, Kelton D, Nielsen SS, Eisenberg S, et al. Control of paratuberculosis: who, why and how. a review of 48 countries. *BMC Vet Res.* 2019;15(1):198.
- Smith RL, Al-Mamun MA, Grohn YT. Economic consequences of paratuberculosis control in dairy cattle: a stochastic modeling study. *Prev Vet Med.* 2017;138:17–27. <https://doi.org/10.1016/j.prevetmed.2017.01.007>.
- Garcia AB, Shalloo L. Invited review: the economic impact and control of paratuberculosis in cattle. *J Dairy Sci.* 2015;98(8):5019–39. <https://doi.org/10.3168/jds.2014-9241>.
- Bach H. *Mycobacterium avium* subsp. *paratuberculosis* play in Crohn's disease? *Curr Infect Dis Rep.* 2015;17(2):463.
- Naser SA, Ghobrial G, Romero C, Valentine JF. Culture of *Mycobacterium avium* subspecies *paratuberculosis* from the blood of patients with Crohn's disease. *The Lancet.* 2004;364(9439):1039–44. [https://doi.org/10.1016/S0140-6736\(04\)17058-x](https://doi.org/10.1016/S0140-6736(04)17058-x).
- Naser SA, Sagrainsingh SR, Naser AS, Thanigachalam S. *Mycobacterium avium* subspecies *paratuberculosis* causes Crohn's disease in some inflammatory bowel disease patients. *World J Gastroenterol.* 2014;20(23):7403–15. <https://doi.org/10.3748/wjg.v20.i23.7403>.
- Bo M, Arru G, Niegowska M, Erre GL, Manchia PA, Sechi LA. Association between lipoprotein levels and humoral reactivity to *Mycobacterium avium* subsp. *paratuberculosis* in multiple sclerosis, type 1 diabetes mellitus and rheumatoid arthritis. *Microorganisms.* 2019;7(10):423.
- Dow CT, Sechi LA. Cows get Crohn's disease and they're giving us diabetes. *Microorganisms.* 2019;7(10):466. <https://doi.org/10.3390/microorganisms7100466>.
- Frau J, Cossu D, Coghe G, Loreface L, Fenu G, Porcu G, et al. Role of interferon-beta in *Mycobacterium avium* subspecies *paratuberculosis* antibody response in Sardinian MS patients. *J Neurol Sci.* 2015;349(1–2):249–50. <https://doi.org/10.1016/j.jns.2015.01.004>.
- Gerrard ZE, Swift BMC, Botsaris G, Davidson RS, Hutchings MR, Huxley JN, et al. Survival of *Mycobacterium avium* subspecies *paratuberculosis* in retail pasteurised milk. *Food Microbiol.* 2018;74:57–63. <https://doi.org/10.1016/j.fm.2018.03.004>.
- Rani S, Beaver A, Schukken YH, Pradhan AK. Modeling the effects of infection status and hygiene practices on *Mycobacterium avium* subspecies *paratuberculosis* contamination in bulk tank milk. *Food Control.* 2019;104:367–76. <https://doi.org/10.1016/j.foodcont.2019.04.031>.
- Chaubey KK, Singh SV, Gupta S, Singh M, Sohal JS, Kumar N, et al. *Mycobacterium avium* subspecies *paratuberculosis* - an important food borne pathogen of high public health significance with special reference to

- India: an update. *Vet Q.* 2017;37(1):282–99. <https://doi.org/10.1080/01652176.2017.1397301>.
17. Singh SV, Kumar N, Sohal JS, Singh AV, Singh PK, Agrawal ND, et al. First mass screening of the human population to estimate the bio-load of *Mycobacterium avium* subspecies *paratuberculosis* in North India. *J Biol Sci.* 2014;14(4):237–47.
 18. Windsor PA, Eppleston J, Dhand NK, Whittington RJ. Effectiveness of Gudair vaccine for the control of ovine John's disease in flocks vaccinating for at least 5 years. *Aust Vet J.* 2014;92(7):263–8. <https://doi.org/10.1111/avj.12194>.
 19. Park HT, Yoo HS. Development of vaccines to *Mycobacterium avium* subsp. *paratuberculosis* infection. *Clin Exp Vaccine Res.* 2016;5(2):108–16. <https://doi.org/10.7774/cevr.2016.5.2.108>.
 20. O'Hagan DT, Rahman D, McGee JP, Jeffery H, Davies MC, Williams P, et al. Biodegradable microparticles as controlled release antigen delivery systems. *Immunology.* 1991;73(2):239–42.
 21. Choi J-S, Seo K, Yoo J-W. Recent advances in PLGA particulate systems for drug delivery. *J Pharm Investig.* 2012;42(3):155–63. <https://doi.org/10.1007/s40005-012-0024-5>.
 22. Allahyari M, Mohit E. Peptide/protein vaccine delivery system based on PLGA particles. *Hum Vaccin Immunother.* 2016;12(3):806–28. <https://doi.org/10.1080/21645515.2015.1102804>.
 23. Ashhurst AS, Parumasivam T, Chan JGY, Lin LCW, Florido M, West NP, et al. PLGA particulate subunit tuberculosis vaccines promote humoral and Th17 responses but do not enhance control of *Mycobacterium tuberculosis* infection. *PLoS One.* 2018;13(3):e0194620.
 24. Destache CJ, Belgium T, Christensen K, Shibata A, Sharma A, Dash A. Combination antiretroviral drugs in PLGA nanoparticle for HIV-1. *BMC Infect Dis.* 2009;9:198. <https://doi.org/10.1186/1471-2334-9-198>.
 25. Ham AS, Cost MR, Sassi AB, Dezzutti CS, Rohan LC. Targeted delivery of PSC-RANTES for HIV-1 prevention using biodegradable nanoparticles. *Pharm Res.* 2009;26(3):502–11. <https://doi.org/10.1007/s11095-008-9765-2>.
 26. Sweeney EE, Balakrishnan PB, Powell AB, Bowen A, Sarabia I, Burga RA, et al. PLGA nanodeposits co-encapsulating prostratin and anti-CD25 enhance primary natural killer cell antiviral and antitumor function. *Nano Res.* 2020;13(3):736–44. <https://doi.org/10.1007/s12274-020-2684-1>.
 27. Tukhvatulin A, Dzharullaeva A, Erokhova A, Zemskaya A, Balyasin M, Ozharovskaia T, et al. Adjuvantation of an influenza hemagglutinin antigen with TLR4 and NOD2 Agonists Encapsulated in Poly(D, L-Lactide-Co-Glycolide) nanoparticles enhances immunogenicity and protection against lethal influenza virus infection in mice. *Vaccines (Basel).* 2020;8(3):519. <https://doi.org/10.3390/vaccines8030519>.
 28. Brooks BW, Young NM, Watson DC, Robertson RH, Sugden EA, Nielsen KH, et al. *Mycobacterium paratuberculosis* antigen D: characterization and evidence that it is a bacterioferritin. *J Clin Microbiol.* 1991;29(8):1652–8.
 29. Lee BY, Horwitz MA, Clemens DL. Identification, recombinant expression, immunolocalization in macrophages, and T-cell responsiveness of the major extracellular proteins of *Francisella tularensis*. *Infect Immun.* 2006;74(7):4002–13. <https://doi.org/10.1128/IAI.00257-06>.
 30. Al-Mariri A, Tibor A, Lestrade P, Mertens P, De Bolle X, Letesson JJ. *Yersinia enterocolitica* as a vehicle for a naked DNA vaccine encoding *Brucella abortus* bacterioferritin or P39 antigen. *Infect Immun.* 2002;70(4):1915–23. <https://doi.org/10.1128/IAI.70.4.1915-1923.2002>.
 31. Al-Mariri A, Tibor A, Mertens P, De Bolle X, Michel P, Godefroid J, et al. Protection of BALB/c mice against *Brucella abortus* 544 challenge by vaccination with bacterioferritin or P39 recombinant proteins with CpG oligodeoxynucleotides as adjuvant. *Infect Immun.* 2001;69(8):4816–22. <https://doi.org/10.1128/IAI.69.8.4816-4822.2001>.
 32. Groenendaal H, Zagmutt FJ, Patton EA, Wells SJ. Cost-benefit analysis of vaccination against *Mycobacterium avium* ssp. *paratuberculosis* in dairy cattle, given its cross-reactivity with tuberculosis tests. *J Dairy Sci.* 2015;98(9):6070–84. <https://doi.org/10.3168/jds.2014-8914>.
 33. Vartak A, Sucheck SJ. Recent advances in subunit vaccine carriers. *Vaccines (Basel).* 2016;4(2):12. <https://doi.org/10.3390/vaccines4020012>.
 34. Moyle PM, Toth I. Modern subunit vaccines: development, components, and research opportunities. *ChemMedChem.* 2013;8(3):360–76. <https://doi.org/10.1002/cmdc.201200487>.
 35. Silva AL, Soema PC, Slutter B, Ossendorp F, Jiskoot W. PLGA particulate delivery systems for subunit vaccines: linking particle properties to immunogenicity. *Hum Vaccin Immunother.* 2016;12(4):1056–69. <https://doi.org/10.1080/21645515.2015.1117714>.
 36. Waeckerle-Men Y, Groettrup M. PLGA microspheres for improved antigen delivery to dendritic cells as cellular vaccines. *Adv Drug Deliv Rev.* 2005;57(3):475–82. <https://doi.org/10.1016/j.addr.2004.09.007>.
 37. Tarhini M, Greige-Gerges H, Elaissari A. Protein-based nanoparticles: from preparation to encapsulation of active molecules. *Int J Pharm.* 2017;522(1–2):172–97. <https://doi.org/10.1016/j.ijpharm.2017.01.067>.
 38. Tooker BC, Burton JL, Coussens PM. Survival tactics of *M. paratuberculosis* in bovine macrophage cells. *Vet Immunol Immunopathol.* 2002;87(3–4):429–37.
 39. Subharat S, Shu D, Wedlock DN, Price-Carter M, de Lisle GW, Luo D, et al. Immune responses associated with progression and control of infection in calves experimentally challenged with *Mycobacterium avium* subsp. *paratuberculosis*. *Vet Immunol Immunopathol.* 2012;149(3–4):225–36. <https://doi.org/10.1016/j.vetimm.2012.07.005>.
 40. Coussens PM, Sipkovsky S, Murphy B, Roussey J, Colvin CJ. Regulatory T cells in cattle and their potential role in bovine paratuberculosis. *Comp Immunol Microbiol Infect Dis.* 2012;35(3):233–9. <https://doi.org/10.1016/j.cimid.2012.01.004>.
 41. Koets A, Rutten V, Hoek A, van Mil F, Muller K, Bakker D, et al. Progressive bovine paratuberculosis is associated with local loss of CD4⁺ T cells, increased frequency of gamma delta T cells, and related changes in T-cell function. *Infect Immun.* 2002;70(7):3856–64. <https://doi.org/10.1128/IAI.70.7.3856-3864.2002>.
 42. Raupach B, Kaufmann S. Immune responses to intracellular bacteria. *Curr Opin Immunol.* 2001;13(4):417–28.
 43. Ottenhoff TH, Boer T, Verhagen CE, Verreck FA, Dissel JT. Human deficiencies in type 1 cytokine receptors reveal the essential role of type 1 cytokines in immunity to intracellular bacteria. *Microbes Infect.* 2000;2(13):1559–66.
 44. Lawlor C, O'Connor G, O'Leary S, Gallagher PJ, Cryan SA, Keane J, et al. Treatment of mycobacterium tuberculosis-infected macrophages with poly(Lactic-Co-Glycolic Acid) microparticles drives NFkappaB and autophagy dependent bacillary killing. *PLoS One.* 2016;11(2):e0149167.
 45. Trinchieri G. Interleukin-10 production by effector T cells: Th1 cells show self control. *J Exp Med.* 2007;204(2):239–43. <https://doi.org/10.1084/jem.20070104>.
 46. Khare G, Nangpal P, Tyagi AK. Differential roles of iron storage proteins in maintaining the iron homeostasis in mycobacterium tuberculosis. *PLoS One.* 2017;12(1):e0169545.
 47. Mohanty A, Subhadarshane B, Barman P, Mahapatra C, Aishwarya B, Behera RK. Iron mineralizing bacterioferritin A from mycobacterium tuberculosis exhibits unique catalase-Dps-like dual activities. *Inorg Chem.* 2019;58(8):4741–52. <https://doi.org/10.1021/acs.inorgchem.8b02758>.
 48. Pandey R, Rodriguez GM. A ferritin mutant of *Mycobacterium tuberculosis* is highly susceptible to killing by antibiotics and is unable to establish a chronic infection in mice. *Infect Immun.* 2012;80(10):3650–9. <https://doi.org/10.1128/IAI.00229-12>.
 49. Elsaghier A, Prantera C, Moreno C, Ivanyi J. Antibodies to *Mycobacterium paratuberculosis*-specific protein antigens in Crohn's disease. *Clin Exp Immunol.* 1992;90:503–8.
 50. Xu Z, Qin Y, Wang Y, Li X, Cao H, Zheng SJ. A critical role of Bacterioferritin in *Salmonella pullorum*-induced IFN-beta expression in DF-1 Cells. *Front Microbiol.* 2016;7:20. <https://doi.org/10.3389/fmicb.2016.00020>.
 51. Satyanarayanan SK, El Kebir D, Soboh S, Butenko S, Sekheri M, Saadi J, et al. IFN-beta is a macrophage-derived effector cytokine facilitating the resolution of bacterial inflammation. *Nat Commun.* 2019;10(1):3471. <https://doi.org/10.1038/s41467-019-10903-9>.
 52. de Weerd NA, Samarajiwu SA, Hertzog PJ. Type I interferon receptors: biochemistry and biological functions. *J Biol Chem.* 2007;282(28):20053–7. <https://doi.org/10.1074/jbc.R700006200>.
 53. Ladero-Aunon I, Molina E, Oyanguren M, Barriales D, Fuertes M, Sevilla IA, et al. Oral vaccination stimulates neutrophil functionality and exerts protection in a *Mycobacterium avium* subsp. *paratuberculosis* infection model. *NPJ Vaccines.* 2021;6(1):102. <https://doi.org/10.1038/s41541-021-00367-8>.
 54. Settles EW, Kink JA, Talaat A. Attenuated strains of *Mycobacterium avium* subspecies *paratuberculosis* as vaccine candidates against John's disease. *Vaccine.* 2014;32(18):2062–9. <https://doi.org/10.1016/j.vaccine.2014.02.010>.

55. Rosseels V, Huygen K. Vaccination against paratuberculosis. *Expert Rev Vaccines*. 2008;7(6):817–32. <https://doi.org/10.1586/14760584.7.6.817>.
56. Yue R, Liu C, Barrow P, Liu F, Cui Y, Yang L, et al. The isolation and molecular characterization of *Mycobacterium avium* subsp. *paratuberculosis* in Shandong province, China. *Gut Pathog*. 2016;8:9. <https://doi.org/10.1186/s13099-016-0092-6>.
57. O'Connor G, Krishnan N, Fagan-Murphy A, Cassidy J, O'Leary S, Robertson BD, et al. Inhalable poly(lactic-co-glycolic acid) (PLGA) microparticles encapsulating all-trans-Retinoic acid (ATRA) as a host-directed, adjunctive treatment for *Mycobacterium tuberculosis* infection. *Eur J Pharm Biopharm*. 2019;134:153–65. <https://doi.org/10.1016/j.ejpb.2018.10.020>.

Publisher's Note

Springer Nature remains neutral with regard to jurisdictional claims in published maps and institutional affiliations.

Ready to submit your research? Choose BMC and benefit from:

- fast, convenient online submission
- thorough peer review by experienced researchers in your field
- rapid publication on acceptance
- support for research data, including large and complex data types
- gold Open Access which fosters wider collaboration and increased citations
- maximum visibility for your research: over 100M website views per year

At BMC, research is always in progress.

Learn more biomedcentral.com/submissions

